RESEARCH ARTICLE

CrossMark

Characterization of Biopolymer-Based UV-Activated Intelligent Oxygen Indicator for Food-Packaging Applications

Gaurav Kr Deshwal[1] · Narender Raju Panjagari[1] · Richa Badola[1] · Ashish Kumar Singh[1] · Prashant Saurabh Minz[1] · Sangita Ganguly[1] · Tanweer Alam[1]

Abstract

An attempt was made in the present study to develop and characterize sodium alginate (SA-MB-NR), sodium caseinate (SC-MB-RSS), and carrageenan (CG-MB) ultraviolet light activated intelligent oxygen indicator. Among all the sensor films, CG-MB displayed least overall migration in all the food simulants. Tensile strength of CG-MB sensor film was found to be the highest among all. FTIR spectra of the original and photo-activated sensor films revealed changes in the alkyl, amide, and hydroxyl groups. Equilibrium moisture content of the sensor films was found to be in the range of 94.73–120.26 g 100 g^{-1}. Peleg model was found to best describe the sorption behaviour of SA-MB-NR while SC-MB-RSS and CG-MB were best described by D'Arcy and Watt model. All the three sensor films were found to be equally sensitive to oxygen concentration varying from 2 to 10% but significantly differed at 1% ($P < 0.05$). All the three sensor films were found to be equally sensitive to oxygen at as low as below 1% concentration. Hence, it can be concluded that film CG-MB could be potentially applied as an oxygen leak indicator for direct contact (vacuum) or non-direct contact (modified atmosphere) food-packaging applications.

Keywords Biopolymer · Oxygen indicator · Colorimetric · Intelligent packaging · Machine vision

Introduction

Intelligent packaging has witnessed significant growth due to newly developed products and their packaging requirements along with consumer preferences over the past decade. Intelligent packaging is defined as a packaging that contains internal or external indicators to provide information about aspects of the history of the package and/or the quality of the food [57]. According to the European Commission (EC/450/2009), intelligent materials and articles are those that monitor the condition of packaged food or the environment surrounding the food. Intelligent packaging market was worth $1400 million in 2008 and is expected to touch the figures of $5300 million in 2017 [8, 54]. Intelligent packaging systems are classified into three categories, namely, sensors, indicators, and radio frequency identification (RFID) systems [9]. Among all these intelligent systems, colorimetric sensors relying on low cost dyes are popular. These sensors indicate the history or quality of the product based on the visual colour change, which can be easily detected by all the stakeholders in the supply chain. With the focal point being shifted to consumer convenience, quality indicators can indicate the quality of the food at the point of sale to consumers.

Oxygen is the major cause of food spoilage, leading to respiration, oxidation of lipids and micronutrients, aerobic microbial growth and objectionable changes in colour, flavour, and odour. Therefore, several food products are subjected to modified atmosphere packaging (MAP) with reduced oxygen in the headspace to increase the shelf life [57] by about 3–4 times as compared to those packaged with atmospheric air [10, 34]. However, MAP dairy products such as Cheddar cheese (N_2:CO_2 70:30) [47], Fiordilatte cheese (N_2:CO_2 50:50) [38], Graviera Agraphon cheese (N_2:CO_2 50:50) [18], *paneer* (N_2:CO_2 50:50) [64], *lal peda* (N_2:CO_2 70:30) [28], dietetic *rabri* (100% N_2) [22] and *Kalakand* (N_2:CO_2 50:50) [27], MAP bakery products such as bread (N_2:CO_2 90:10) [24] (N_2:CO_2 70:30) [45] and MAP cooked chicken patties (N_2:CO_2 70:30) [62], raw, and cooked beef (N_2:CO_2 60:40) [61] do not contain oxygen in the headspace. Studies have reported that the residual oxygen content of

✉ Narender Raju Panjagari
  pnr.ndri@gmail.com

1 Food Packaging Laboratory, Dairy Technology Division, ICAR-National Dairy Research Institute, Karnal, Haryana 132001, India

MAP food products such as cooked chicken patties [62], raw and cooked beef [61], and cheese [47] slightly increases during storage. The changes in the headspace oxygen concentration during storage could be either due to the loss of seal integrity, presence of pinholes, or oxygen permeability of the packaging material, leading to ingress of oxygen. This may affect the product quality in terms of microbial growth and reduced shelf life.

Although oxygen sensors have been developed based on the several mechanisms (fluorescence, conductance, and luminescence), such sensors are costly, require trained manpower to operate, lack portability [53], and are unsuitable for food-packaging applications. The colorimetric oxygen sensors could be efficiently used as the simplest package integrity indicator providing information about the opening of the package or ingress of oxygen or inefficient atmosphere modification around the product in MAP systems. Among all types of product quality indicators, the colorimetric oxygen indicators are the most commonly used ones with MAP food products [68], which comprise of a redox dye, a reducing agent, a photo-catalyst, and an encapsulating polymer [40].

For producers to deliver high-quality MAP dairy products with proper indication of its quality at the point of sale, there is a need for a sensor, which can detect oxygen. However, the dye-based oxygen sensors available in the market are lacking biopolymer-based encapsulating agent for binding the components of the sensor so as to be compatible with dairy and food products. Limited studies have been conducted in this area but characterization of such oxygen sensors have not been studied in detail. Hence, the aim of the present study is to develop biopolymer-based oxygen leak indicator and characterization of such sensors for potential food-packaging applications.

Materials and Methods

Preparation of Biopolymer-Based Sensor Films

In the present study, three different biopolymers such as sodium caseinate (90% on db, M/s Mahaan Proteins Ltd., Kosi Kalan, Mathura, India), sodium alginate (M/s Sigma-Aldrich, St. Louis, USA), and kappa carrageenan (M/s Sigma-Aldrich, St. Louis, USA) were used. The sodium caseinate (SC-MB-RSS), sodium alginate (SA-MB-NR), and carrageenan (CG-MB) based films were prepared as per the methods given by Kristo [31], Tavassoli-Kafrani and co-workers [63] and Cha and co-workers [11], respectively, with some minor modifications. Based on some preliminary trials, the levels of methylene blue (MB), resazurin sodium salt (RSS), neutral red (NR), titanium dioxide, and glycerol used in the study have been decided. The details of the formulation are given in Table 1. The aqueous solutions of the respective biopolymers were prepared by dissolving the

Table 1 Components used for biopolymer-based sensor film fabrication

Sensor film components (g/100 mL water)	Type of sensor film		
	SC-MB-RSS	SA-MB-NR	CG-MB
Sodium caseinate	8	–	–
Sodium alginate	–	4	–
Carrageenan	–	–	1
Methylene blue	0.12	0.12	0.12
Resazurin sodium salt	0.12	–	–
Neutral red	–	0.12	–
Glycerol	7.2	7.2	7.2
Titanium dioxide	7.2	7.2	7.2

selected quantities of biopolymer (Table 1) in distilled water to which glycerol and titanium dioxide were added. Later, the respective selected dyes were mixed with the polymer solutions. The prepared solutions were continuously stirred (600 rpm) using a magnetic stirrer (Digital Spinot, M/s Tarsons Pvt. Ltd.) for complete hydration and dissolution, followed by casting and drying at 35–40 °C for 6–8 h. SC-MB-RSS and SA-MB-NR solutions were mixed at 35 °C for 1–2 h and 4–5 h, respectively, while CG-MB solution was mixed at 75–80 °C for 30 min. The foam generated during mixing was siphoned off before casting the film solutions.

Mechanical and Spectral Properties

Mechanical properties, namely, thickness, tensile strength, and percent elongation at break of all the three sensor films, were determined. Thicknesses of sensor films were determined using a digital micrometer (M/s Engineering Corporation, Saharanpur, Uttar Pradesh). Thickness of each sample was measured at 20 random positions across the film (10×10 cm^2) and the mean value was calculated and expressed in microns. The tensile strength and elongation at break of the films were measured using a Texture Analyzer (TA.XT2i, M/s Stable Micro System, UK), fitted with 25 kg load cell, according to ASTM standard method D882 [4]. Before testing, all samples were equilibrated at $50 \pm 2\%$ relative humidity and 37 °C for 2 days. Prior to the test, film samples were cut into rectangular strips with dimension of 2.54 cm $\times$ 10 cm. The initial grip separation was set at 50 mm and crosshead speed at 2 mm/s. The test was repeated with ten sensor film specimens. Tensile strength and elongation at break of the sensor film were calculated as follows:

Tensile strength (MPa)

$$= \frac{\text{Load at break (N)}}{\text{Original width (mm)} \times \text{Original thickness (mm)}} \quad (1)$$

$$\text{Elongation at break (\%)} = \frac{\text{Elongation at rupture (mm)}}{\text{Initial gauge length (mm)}} \times 100. \quad (2)$$

Puncture strength was determined using the texture analyzer (TA.XT2i) and expressed in Newton (N). The Fourier transform infrared spectroscopy (FTIR) spectrum of the developed sensor film was recorded using a spectrophotometer (Model: IRAffinity-1 CE, Make: Shimadzu, Japan). The film was mounted directly in the sample holder and spectra of the films were recorded at room temperature over a wave numbers ranged from 400 to 4000 cm^{-1} with a resolution of 4 cm^{-1} and averaged over 30 scans.

Overall Migration into Food Simulants

Overall or global migration from the developed sensor films was determined according to the Bureau of Indian Standards [26] specifications. Five different food simulants such as distilled water, acetic acid (3%, w/v), ethanol (10% v/v and 50% v/v), and n-heptane were used. Sensor film sample of 50 cm^2 (5 cm × 5 cm × 2 sides) surface area was exposed to the simulant on both sides. Three replicates and one blank for each type of simulant were considered. Cylindrical bottles of 100 mL capacity were filled with the required quantity of preheated simulants at the test temperature (38 °C for n-heptane and 40 °C for rest of the simulants). Test specimens were immersed in the simulant completely and covered with threaded screw caps. These samples were then placed in a BOD incubator at the prescribed temperature for the prescribed length of time, namely, 38 °C/30 min for n-heptane and 40 °C/10 days for rest of the simulants. At the end of the test period, samples were removed with the help of a glass rod and washed with small quantity of fresh simulant and combined with the extractants. The extracted simulants were concentrated to 5–6 mL, by evaporating on a hot plate under low heat (n-heptane was concentrated by distillation). These concentrates were transferred into clean-tarred stainless steel dishes along with three washings with small amount of fresh simulant and further evaporated to dryness in an oven maintained at 100 ± 5 °C. After evaporation, these dishes were cooled in a desiccator for 30 min and weighed to nearest 0.1 mg until constant weight of the residue was obtained. The extractive was calculated and expressed in mg/dm^2 using Eq. (3). Blanks were carried out without the samples. Heptane extractive values were divided by factor of five for arriving at the extractivity of a food product as given in BIS specifications. The migration of MB dye from all the sensor films into distilled water was determined by measuring the absorbance at λ_{max} at 661 nm [42]:

$$\text{Amount of extractive (Ex)} = \frac{M}{A} \times 100 \text{ mg/dm}^2 \qquad (3)$$

where $M =$ mass of residue in "mg" minus blank value and $A =$ total surface area in "cm^2" exposed in each replicate.

Water Sorption Behaviour and its Modeling

The moisture sorption isotherms of the sensor films were determined by the static method at 25 °C as per the method given by Panjagari and co-workers [48]. Ten sorption apparatus (sorbostats) with saturated salt solutions such as LiCl, CH_3COOK, $MgCl_2$, K_2CO_3, $Mg(NO_3)_2$, $NaNO_3$, NaCl, KCl, and KNO_3 were prepared, with the water activity of 0.114, 0.237, 0.328, 0.443, 0.536, 0.658, 0.761, 0.855, and 0.923, respectively. Sorbostats were allowed to equilibrate for 7 days before samples were placed into them. The film samples were cut (1 cm × 1 cm) and stored in a desiccator containing phosphorous pentoxide for 2 days at 25 °C. Weighed quantity of dried film samples (200–300 mg) was taken into tared sample beakers and then transferred to the sorbostats. The film samples were weighed at 2-day interval until there was no discernable weight change after attaining equilibrium. The study was repeated with triplicate samples and expressed as equilibrium moisture content (EMC) (g water/100 g solids). The EMCs were plotted against relative humidity to establish moisture sorption isotherms and four different models (Table 2) were used to describe the sorption behaviour. The constants of the sorption models were estimated using nonlinear regression function of OriginPro 8 software.

Table 2 Moisture sorption models used for fitting experimental data

Name of the model	Equation	References
Three-parameter models		
Park	$C = \frac{A_L b_L a_w}{1 + b_L a_w} + K_H a_w + K_a n a_w^n$	Belbekhouche et al. [7]
Ferro-Fontan	$M = \left[\frac{B}{\text{Ln}(A/a_w)}\right]^C$	Fontan et al. [19]
Four-parameter model		
Peleg	$M = A(a_w)^{C_1} + B(a_w)^{C_2}$	Peleg [50]
Five-parameter model		
D'Arcy and Watt	$M = \frac{K_1 K_2 a_w}{1 + K_1 a_w} + K_3 a_w + \frac{K_4 K_5 a_w}{1 - K_4 a_w}$	D'Arcy and Watt [14]

Loading of Sensor Tags on MAP Trays for O_2 Sensitivity

The developed sensor films were tested for their sensitivity towards different concentrations of oxygen (1–10%) for which the sensor films were cut into small tags of 1×1 cm^2 and affixed on the sealant high barrier plastic film from inside of the MAP trays. Polystyrene (PS) trays (LWH, $203 \times 146 \times 60$ mm; thickness: 500 μ) procured from M/s Elixir Technologies, Bengaluru, India were used for this purpose. Ethylene vinyl alcohol (EVOH) films procured form M/s Alpha Packaging Pvt. Ltd., New Delhi, India were used for sealing the trays. The thickness, water vapour transmission rate (WVTR), and oxygen transmission rate (OTR) of EVOH films were 110 μ, 7.89 g/m^2 day (38 °C, 90% RH), and 0.035 mL/m^2 day (23 °C, 0% RH), respectively. For determining the sensitivity of the sensor films, MAP tray-sealing machine (Vac-Star, S220 SP) procured from Elixir Technologies, Bengaluru, India was used which has a PLC-based programming system. The tray-sealing chamber was first evacuated and flushed with desired gas composition (N_2: 90–99%; O_2: 1–10%). The nitrogen and oxygen cylinders were procured from local market and used for mixing of gases in a gas-mixing device (Mix 9001 ME) attached with the system. The headspace gas composition inside the MAP trays after the operation was determined using a headspace analyser purchased from PBI Dansensor (CheckMate 9900), Denmark.

UV Activation and Colour Vision System

A wooden cabinet ($46 \times 43 \times 50$ cm) fitted with two short wave UV lights (30 cm long, 254 nm, Make: Philips, TUV 16W, G16 T5) separated at a distance of 18 cm on the inner top side along with LED wall light (fixed at a height of 33 cm) was fabricated and used as UV treatment chamber for photoactivation of the sensor films. Distance between the sensor film and UV tubes was maintained at 15 cm. Digital camera lens axis and the lightning source were fixed at an angle of 45°, because the phenomenon of diffuse reflection responsible for the colour occurs at 45° from the incident light [20]. LED wall light (Philips™, $137 \times 239 \times 37$ mm; 10 W) was used as the light source (cool white light 6500 K; light flux of 500 lm) with good colour rendering index (CRI) or colour accuracy of 80. The image of the sensor film was captured by digital camera (Model-EOS 450D, Canon) with a resolution of 4272×2848, which is equivalent to 12.2 megapixel. All the three stages of sensor film, namely, original (non-UV treated), UV treated, and recovered (films exposed to ambient oxygen for regaining of colour) images, were acquired and transferred to a computer system for further analysis. The quantitative colour values of the acquired images were determined using Adobe Photoshop CS6

Extended software (version 6.2). The software displays colour values in several formats (*Lab*, RGB and CMYK) in the info palette and histogram window. Since CIE ($L*$, $a*$, and $b*$) values are device independent and cover a larger gamut than RGB and CMYK [58], the acquired images colour values were converted to standard colour ($L*$, $a*$ and $b*$) values using the following formulas [32]:

$$L^* = \frac{L}{255} \times 100 \tag{4}$$

$$a^* = \frac{240a - 120}{510} \times 100 \tag{5}$$

$$b^* = \frac{240b - 120}{510} \times 100. \tag{6}$$

Statistical Analysis

The goodness of fit of different sorption models was determined by multiple statistical criteria such as coefficient of determination (R^2), reduced Chi square (χ^2), percent mean deviation error (P), and root mean square error percent (RMS%) using Eqs. (7–10) given below. The data obtained the study were subjected to one-way ANOVA using SAS Enterprise Guide (version 4.3) (Cary, NC, USA):

$$R^2 = \frac{\sum_{i=1}^{n} \left(M_{pre} - \bar{M}\right)^2}{\sum_{i=1}^{n} \left(M_{exp} - \bar{M}\right)^2} \tag{7}$$

$$\chi^2 = \frac{1}{N-n} \sum_{i=1}^{N} \left(M_{exp} - M_{pre}\right)^2 \tag{8}$$

$$P = \frac{100}{n} \sum_{i=1}^{n} \left| \frac{M_{i\,exp} - M_{ipre}}{M_{i\,exp}} \right| \tag{9}$$

$$RMS\% = \sqrt{\frac{1}{n} \left[\sum_{1}^{n} \left(\frac{M_{exp} - M_{pre}}{M_{exp}} \right)^2 \right]} \times 100 \tag{10}$$

Results and Discussion

Mechanical Properties

The mechanical properties of the developed films in terms of tensile strength, percent elongation, puncture resistance, and thickness are presented in Table 3. The carrageenan-based sensor film was having the lowest thickness and highest tensile strength, while the highest elongation at break

Table 3 Mechanical properties and overall migration of the sensor films

Properties/simulant	Biopolymer-based sensor film		
	SA-MB-NR	SC-MB-RSS	CG-MB
Mechanical properties			
Thickness (μm)	149 ± 0.01^{A}	146 ± 0.01^{A}	129 ± 0.04^{A}
Tensile strength (MPa)	0.56 ± 0.09^{A}	0.45 ± 0.03^{A}	1.33 ± 0.45^{B}
Elongation at break (%)	0.34 ± 0.09^{A}	0.40 ± 0.13^{A}	0.34 ± 0.09^{A}
Puncture strength (N)	0.93 ± 0.34^{B}	0.24 ± 0.04^{A}	0.21 ± 0.03^{A}
Overall migration (mg/dm^2)			
Distilled water	550.77 ± 10.01^{aA}	620.59 ± 9.85^{aB}	22.38 ± 1.05^{aC}
3% acetic acid	580.59 ± 9.89^{aA}	510.50 ± 9.56^{bB}	36.41 ± 0.98^{bC}
10% ethanol	890.48 ± 10.11^{bA}	735.32 ± 5.04^{cB}	14.28 ± 0.07^{cC}
50% ethanol	740.78 ± 19.98^{cA}	835.74 ± 4.93^{dB}	14.48 ± 0.25^{cC}
n-Heptane	5.24 ± 0.8^{dA}	7.38 ± 1.38^{eA}	4.25 ± 0.15^{dA}

Mean ± SD

[abcde]Values with different superscripts within a column within a property represents significant difference ($P < 0.05$)

[ABC]Values with different superscripts within a row represents significant difference ($P < 0.05$)

was observed for SC-MB-RSS. All the three films were very sticky which could be attributed to the presence of higher amount of glycerol [59]. However, SA-MB-NR and SC-MB-RSS sensor films were observed to be smooth and shiny, while the CG-MB was rough. Roughness of the carrageenan-based sensor could be due to formation of a gel solution on mixing all the ingredients. Sodium alginate sensor film was observed to have a thickness of 149 ± 0.01 μm, while tensile strength was 0.56 ± 0.09 MPa, elongation at break was 0.34 ± 0.09%, and puncture strength was 0.93 ± 0.34 N. All the mechanical properties were observed to be very low except for thickness, which was on the higher side when compared with other films having only sodium alginate and glycerol as main component [55]. The higher thickness could be due to more volume of solution used for casting. The lower values of tensile strength and elongation at break could be due to poor interaction between the various components of the sensor film. Rhim [55] found that the thickness, tensile strength, and elongation at break of sodium alginate-based biodegradable film were 62.9 μm, 33.6 MPa, and 14.0%, respectively. Films prepared by mixing sodium alginate (1.25%) with calcium chloride (1%) and glycerol as plasticizer (50% w/w of polysaccharide) were having a thickness of 12.5 μm, tensile strength 35.0 MPa and elongation at break 8.6%. It was reported that when sodium alginate was mixed with pectin, an increase in tensile strength and elongation at break values was obtained due to better compatibility and stronger chemical interaction between different film components. Sodium alginate–gelatin [67] and alginate and *k*-carrageenan films [49] were having higher elongation at break owing to stronger interaction between the components of the film. The films prepared by dissolving 1% carrageenan in distilled water and using glycerol (50%
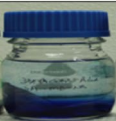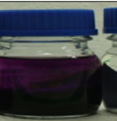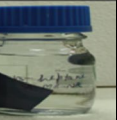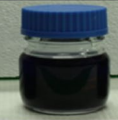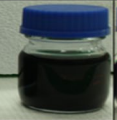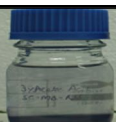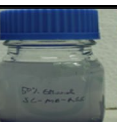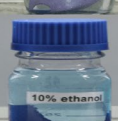
w/w of carrageenan) as plasticizer were having the thickness of 31.33 ± 1.15 μm, while the tensile strength and elongation at break were 26.29 ± 2.93 MPa, 36.46 ± 1.04% respectively [59]. It was reported that higher concentration of glycerol led to sticky and wet films. Rhim [56] reported that the thickness, tensile strength, and elongation at break of carrageenan-based biodegradable film were 58.2 μm, 82.9 MPa, and 4.52%, respectively. The sodium caseinate-based sensor film (SC-MB-RSS) was observed to follow similar trend in the mechanical properties with very low tensile strength, elongation at break, puncture strength, and high thickness. Pereda and co-workers [52] reported a decrease in elastic modulus of caseinate films from 2908 to 250.9 MPa and increase in ultimate elongation from 4 to 63.2% on addition of 28% wt (per cent) of glycerol. The plasticization effect of glycerol was found to be the possible reason for this behaviour. Glycerol reduced the viscosity of sodium caseinate solutions lesser than polyethylene glycol (PEG) due to the changes in the conformation of sodium caseinate chains and protein plasticizer aggregate size. Furthermore, glycerol was reported to affect the tensile strength of the film more than PEG [60]. All these changes can be attributed to the protein-plasticizer and protein–protein interactions and the differences in plasticizer sizes. Audic and Chaufer [5] compared the mechanical performance of sodium caseinate films having different concentrations of plasticizer and reported that the tensile strength decreased and elongation at break increased with increase in the amount of plasticizer (glycerol). The decrease in tensile strength was due to the reduction in the number of interactions between protein chains. In the present study, the poor tensile strength of the developed films could be attributed to the presence of good amount of glycerol in the films.

Overall Migration into Food Simulants

The total amount of solids migrated from the sensor into the food simulants is given in Table 3 and was found to be minimum in n-heptane (4.25 ± 0.15 mg/dm^2) for CG-MB and maximum in 10% ethanol (890.48 ± 10.11 mg/dm^2) for SA-MB-NR. Both SA-MB-NR and SC-MB-RSS sensor films dissolved completely in the food simulants and at the end of the stipulated period of 10 days, they could not be recovered. Migration into all the solvents except n-heptane was more than the prescribed limits by the Bureau of Indian Standards [26]. Among all, the migration of CG-MB film components into n-heptane was very low. Relatively high amount of migration of components from developed films into distilled water, 3% acetic acid, 10% ethanol, and 50% ethanol as compared to n-heptane might be due to the hydrophilic nature of the film components. The CG-MB sensor film could be completely

recovered after 10 days. However, SA-MB-NR and SC-MB-RSS could not be recovered completely. Due to the dissolution of SA-MB-NR and SC-MB-RSS films in all the food simulants (except n-heptane), the colour of the food simulant became completely dark (Fig. 1). Less migration of CG-MB film components could be attributed to the interaction between sulphate moiety of the carrageenan and cationic dye methylene blue [66]. It has been reported that the extent of interaction is also affected by the type of carrageenan [lambda (λ), iota (ι), and kappa (κ)] and also by the sulphate content of these sources. The sulphate content of kappa and lambda carrageenan is 22 and 32% (w/w), respectively [63]. Sulphate groups are responsible for the negative charge of carrageenan and methylene blue is cationic in water. In another study, Vu and Won [65] developed a sensor film containing thionine, glycerol, and TiO$_2$ encapsulated in zein and reported that immersion of film in water for 24 h resulted in 81%

Fig. 1 Images showing the migration of sensor film constituents into different food simulants

Sensor Film / Storage Interval	Food Simulants				
	Distilled Water	Acetic Acid (3%)	Ethanol (10%)	Ethanol (50%)	*n*-Heptane
SA-MB-NR					
Day1					
Day 10 *					
SC-MB-RSS					
Day1					
Day 10 *					
CG-MB					
Day1					
Day 10 *					

* Samples were immersed in *n*-heptane simulant for only 30 minutes as prescribed in IS: 9845 (1998)

dye leaching. However, when alginate was used as an encapsulating polymer the dye leakage reduced to about 6%, which was attributed to the interaction between the cationic dye (thionine) and anionic alginate.

In the present study, the leakage behaviour of MB was studied by spectrophotometry and quantified. It was observed that at the end of 24 h exposure time, the absorbance (OD) values of SA-MB-NR and SC-MB-RSS were found to be 3. Since the Beer Lambert's law does not hold for values greater than 1, the percentage migration of methylene blue dye from SA-MB-NR and SC-MB-RSS could not be calculated. While for CG-MB-based sensor film the absorbance increased from 0.086 to 0.088 during first 3 h and then remained constant at 0.092 until 24 h which was corresponding to 3.55% of MB migration. However, Vu and Won [66] reported that when water-soluble carrageenan (0.2%) was used only 2.1% of MB leached into the water. The lower percentage of dye migration could be attributed to the strong electrostatic interaction of differently charged anionic CG and MB.

Spectral Analysis Using FTIR Spectroscopy

The FTIR absorbance spectrum of SA-MB-NR, SC-MB-RSS, and CG-MB films in original and photo-activated states is presented in Fig. 2. The original and photo-activated curves were overlapped with differences in certain regions. It can be seen from the figure that a visible change in the original and photo-activated sensor film absorbance pattern of SA-MB-NR, SC-MB-RSS, and CG-MB films was observed between the wavenumbers 2300–2500 cm^{-1}. However, the height of the peaks is not same among all the films. Yin and co-workers [69] reported that on mixing two or more substances, in total, different spectra bands are observed due to the changes in the chemical interactions. In the present study, the changes in the spectra of the original and photo-activated films could be ascribed to the presence of different redox dyes and also different biopolymers in the three sensor films. It was reported that when titanium dioxide in nanocrystalline form with a particle size of below 20 nm was used, its coordination with other components changed from octahedral to pentahedral, which was more reactive [15]. Mihailovic and co-workers [39] reported that sodium alginate and titanium atom interaction got enhanced due to the penta-coordinated sites, which resulted in decreased UV transmission, indicating high UV absorption ability of TiO$_2$. In the present study, the clear difference in the peaks of SA-MB-NR and SC-MB-RSS films up on photo-activation could be ascribed to the presence of higher amount of TiO$_2$ and its conformational changes to pentahedral coordination. However, similar effect
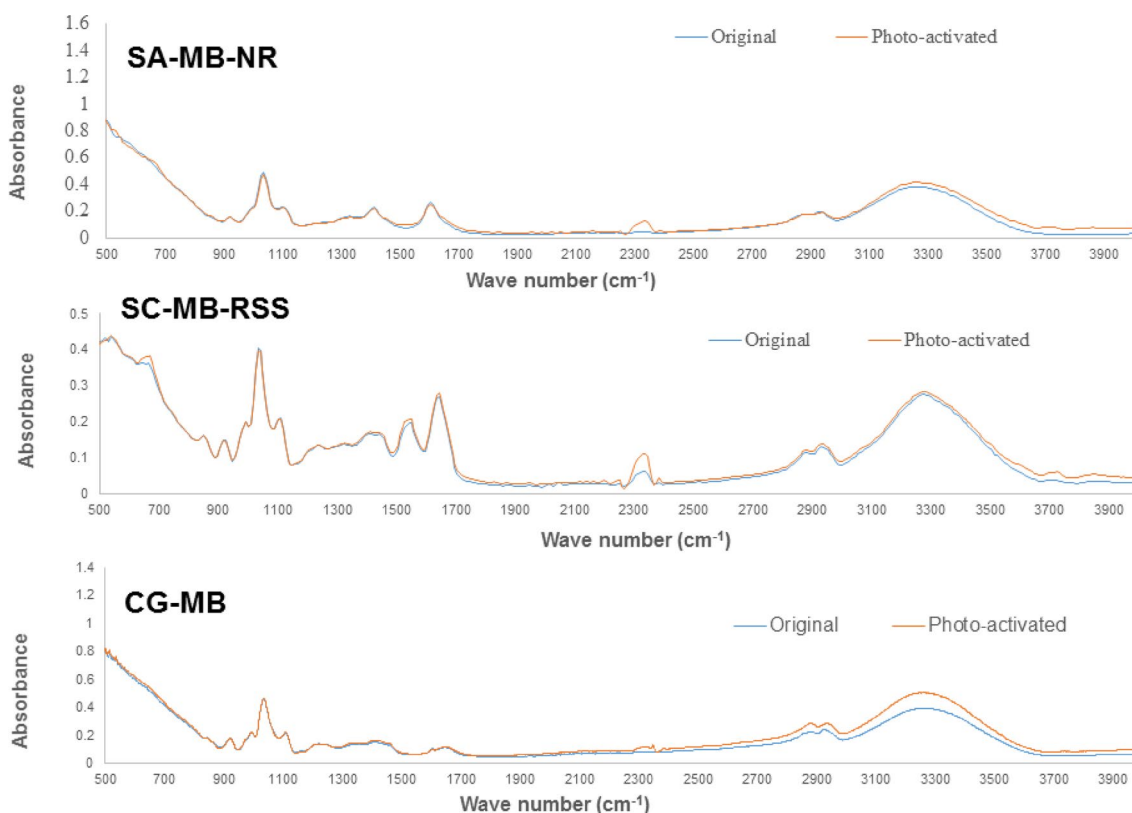

Fig. 2 FTIR absorbance spectra of three biopolymer-based sensor films

was not observed in CG-MB, although TiO_2 was present in the same amount and the reasons for this need to be explored further. Sodium caseinate can form large number of intermolecular hydrogen bonds due to its irregular coiled structure. Blending of sodium caseinate with glycerol is reported to result in an increase in the macromolecular cohesion [6]. The broad absorption difference observed in the SC-MB-RSS film in the 2300–2500 cm^{-1} range could be due to the hydrogen bonds formed between sodium caseinate and glycerol hydroxyl groups [3]. Pereda and co-workers [51] observed different FTIR curves for sodium caseinate–starch blended film as compared to the neat sodium caseinate film. For starch-based material, the absorption bands from 763 to 1136 cm^{-1} reflected the stretching of the C–O bond, while the bands in the 1600–1500 cm^{-1} region were reported to represent the amide-I and amide-II bands common to proteins [52]. However, in the CG-MB, a change was observed due to photo-activation between the wave numbers 2300–3900 cm^{-1} (Fig. 2). Abad and co-workers [1] reported that the spectra of kappa-carrageenan irradiated at 100 kGy in powder form showed no significant change in the functional group with the entire structure remaining intact. However, new absorption band at 1728 cm^{-1} was observed due to increase in UV absorption at 260 nm, which suggested the formation of carbonyl groups. In the present study, the changes in the absorbance spectra of the CG-MB films in the range of 3000–3600 cm^{-1} wave numbers could be due to the stretching of hydroxyl groups (–OH) [46].

Sensitivity of the Selected Films Towards Different Level of Oxygen

SA-MB-NR, SC-MB-RSS, and CG-MB were tested for their sensitivity to different concentrations of oxygen (1–10%) and its effect on the visual appearance, photo-activation time, colour recovery time, and instrumental colour are presented in Fig. 3 In general, the photo-activation time of the sensor films was observed to be in the range of 3–8 min whereas the colour recovery times were found to be in the range of 15–60 min. It can be seen from Tables 4, 5 and 6 that at the lowest concentration of oxygen, the instrumental colour values ($L*$, $a*$, $b*$) of all the three sensor films prior to photo-activation (original) were significantly ($P < 0.05$) different from the rest of the concentrations (2–10%). The $L*$, $a*$, and $b*$ values of SA-MB-NR, SC-MB-RSS, and CG-MB exposed to different levels of oxygen and as affected by photo-activation and recovery are given in Table 4, 5, and 6, respectively. The lightness value of the native SA-MB-NR film (prior to photo-activation) (L_o*) when exposed to 0.6% (1%) oxygen was observed to be 9.26. With an increase in the oxygen concentration from 1 to 2%, L_o* value significantly ($P < 0.05$) increased to 11.57. However, with further increase in oxygen concentration from 3 to 10% no significant change ($P > 0.05$) in L_o* values were observed. Up on photo-activation, the lightness values (L_p*) significantly ($P < 0.05$) increased. It can be seen from Table 4 that across most of the oxygen concentrations, non-significant ($P > 0.05$) differences between the lightness values of the

Oxygen Concentration # (%)	SA-MB-NR			SC-MB-RSS			CG-MB		
	Original Colour	Photo-activated Colour	Recovered Colour	Original Colour	Photo-activated Colour	Recovered Colour	Original Colour	Photo-activated Colour	Recovered Colour
1									
2									
3									
4									
5									
6									
7									
8									
9									
10									

Values represent rounded concentration while within the parenthesis actual oxygen concentration is given.

Fig. 3 Effect of oxygen concentration on the visible colour of original, UV-activated and recovered different sensor films

Table 4 Effect of oxygen concentration on the instrumental colour values of original, photo-activated, and colour-recovered SA-MB-NR film

Oxygen concentration %[1]	Lightness (L*)			Redness (a*)			Blueness (b*)		
	L_o*	L_p*	L_r*	a_o*	a_p*	a_r*	b_o*	b_p*	b_r*
1	9.26±0.77[aA]	12.86±0.52[bB]	8.94±0.67[aA]	3.91±0.94[aA]	6.16±0.76[bcB]	3.67±0.87[aA]	−5.84±1.02[aA]	1.32±0.22[cB]	−5.51±1.07[aA]
2	11.57±0.40[bA]	20.16±0.50[eC]	15.10±0.95[fB]	3.91±0.51[aA]	5.93±0.44[bB]	3.67±0.52[aA]	−5.84±0.68[aA]	0.66±0.14[bcB]	−5.60±0.38[aA]
3	11.57±0.66[bA]	15.29±0.96[cdC]	13.45±0.80[eB]	3.81±0.67[aA]	5.51±0.78[abB]	3.67±0.63[aA]	−5.74±0.47[aA]	0.61±0.55[bB]	−5.60±0.52[aA]
4	11.41±0.27[bA]	15.14±0.59[cdB]	13.02±0.70[eC]	3.67±0.47[aA]	5.18±0.57[abB]	3.53±0.42[aA]	−5.69±0.52[aA]	−0.28±0.68[aC]	−5.18±0.32[aB]
5	11.65±0.82[bA]	15.88±0.81[dC]	13.25±0.89[eB]	3.76±0.32[aA]	5.51±0.59[abB]	3.53±0.21[aA]	−5.79±0.28[aA]	0.80±0.46[bcB]	−5.74±0.37[aA]
6	11.49±0.61[bA]	15.25±0.57[cdB]	11.41±0.69[cdA]	3.95±0.25[aA]	5.65±0.43[abC]	3.62±0.28[aB]	−5.88±0.56[aA]	0.61±0.41[bB]	−5.79±0.51[aA]
7	11.57±0.47[bA]	15.69±0.43[cdB]	12.00±0.71[dA]	3.81±0.38[aA]	5.74±0.70[abB]	3.67±0.30[aA]	−5.84±0.53[aA]	0.66±0.33[bcB]	−5.65±0.82[aA]
8	11.33±0.71[bA]	13.41±0.76[bB]	10.75±0.26[cA]	3.72±0.56[aA]	5.74±1.01[abB]	3.62±0.19[aA]	−5.51±0.55[aA]	2.31±0.74 [dB]	−5.51±0.51[aA]
9	11.61±0.96[bB]	11.88±0.50[aB]	9.65±0.86[bA]	3.72±0.74[aA]	5.65±0.67[abB]	3.62±0.46[aA]	−5.74±0.79[aA]	0.61±1.42[bA]	−5.60±0.82[aA]
10	11.06±0.46[bA]	15.65±0.57[cdC]	8.67±0.69[aB]	3.76±0.48[aA]	6.64±0.67 [dB]	3.62±0.66[aA]	−5.69±0.97[aA]	0.75±0.37[bcB]	−5.55±0.73[aA]

Mean±SD ($n = 16$)

[ABC] Values within a colour attribute (L*, a*, b*) with at least one similar superscript do not differ significantly ($P > 0.05$)

[abcdef] Values within a column with at least one similar superscript don't differ significantly ($P > 0.05$)

[1] Values represent rounded concentration while within the parenthesis actual oxygen concentration is given

Table 5 Effect of oxygen concentration on the instrumental colour values of original, photo-activated, and colour-recovered SC-MB-RSS film

Oxygen concentration (%)[1]	Lightness (L*)			Redness (a*)			Blueness (b*)		
	L_o*	L_p*	L_r*	a_o*	a_p*	a_r*	b_o*	b_p*	b_r*
1 (0.60)	4.43±0.58[aA]	6.51±0.56[aB]	4.51±0.61[aA]	3.44±0.75[aA]	9.18±1.03[bB]	3.86±0.63[bA]	−11.76±2.32[bA]	−10.73±1.30[bA]	−12.28±2.44[aA]
2 (1.81)	7.25±1.68[bA]	7.10±0.77[aA]	8.20±0.62[aB]	3.62±0.66[aA]	7.62±0.76[aB]	3.39±0.52[aA]	−13.79±0.94[aA]	−12.61±1.36[aB]	−12.28±0.79[aB]
3 (2.51)	7.02±0.64[bA]	6.71±1.39[aA]	6.78±0.43[bA]	3.67±0.52[aA]	7.48±0.90[aB]	3.53±0.89[aA]	−13.18±0.71[aA]	−11.25±0.85[bB]	−12.52±0.49[aA]
4 (3.96)	6.98±0.49[bA]	7.18±0.96[aA]	7.53±0.60[cA]	3.53±0.42[aA]	7.44±0.87[aC]	4.19±0.38[bB]	−13.46±0.61[aA]	−12.24±0.57[aB]	−12.52±0.33[aB]
5 (4.64)	6.94±0.35[bB]	6.51±0.36[aA]	6.98±0.55[bB]	3.53±0.21[aA]	7.25±0.65[aB]	3.48±0.33[bA]	−13.18±0.64[aA]	−12.42±0.57[aB]	−12.19±0.43[aB]
6 (6.02)	7.14±0.52[bA]	6.75±0.80[aA]	7.22±0.64[baA]	3.62±0.35[aA]	7.20±1.26[aB]	3.58±0.14[bA]	−13.69±0.74[aA]	−12.14±0.99[aB]	−12.47±0.70[aB]
7 (6.84)	6.94±0.53[bA]	6.55±0.66[aA]	6.90±0.40[bA]	3.62±0.46[aA]	7.11±0.56[aB]	3.58±0.33[bA]	−13.32±0.59[aA]	−12.24±1.14[aB]	−12.24±0.57[aB]
8 (7.72)	7.02±0.51[bA]	6.55±0.66[aA]	7.02±0.45[bA]	3.67±0.30[aA]	7.34±0.83[aB]	3.53±0.21[bA]	−13.69±0.74[aA]	−12.19±0.56[aB]	−12.47±0.84[aB]
9 (8.52)	6.94±0.58[bA]	6.63±0.27[aA]	6.90±0.26[bA]	3.67±0.56[aA]	7.25±0.88[aB]	3.58±0.53[bA]	−13.22±0.76[aA]	−12.28±0.87[aB]	−12.28±0.70[aB]
10 (9.44)	6.98±0.42[bA]	6.78±0.56[aA]	6.82±0.40[bA]	3.58±1.04[aA]	7.58±0.67[aB]	3.48±0.77[bA]	−13.18±0.85[aA]	−12.42±0.39[aA]	−12.38±1.05[aA]

Mean±SD ($n = 16$)

[ABC] Values within a colour attribute (L*, a*, b*) with at least one similar superscript do not differ significantly ($P > 0.05$)

[abc] Values within a column with at least one similar superscript don't differ significantly ($P > 0.05$)

[1] Values represent rounded concentration while within the parenthesis actual oxygen concentration is given

original film (L_o*) and colour-recovered film (L_r*) was observed. However, it was observed that some of the films took as high as 60 min to regain (recover) the original colour. It can be seen from Table 4 that significant differences ($P < 0.05$) in the redness values of the original SA-MB-NR film (a_o*) and the photo-activated SA-MB-NR films (a_p*) exist which almost doubled with photo-activation. Furthermore, it can be seen that up on exposure to ambient air, no significant differences were observed between a_o* and the redness values of the recovered films (a_r*). Similar trends were observed in the original (b_o*), photo-activated (b_p*) and recovered (b_r*) blueness values of SA-MB-NR films.

When exposed to 0.6% (1%) oxygen, the lightness values of the original SC-MB-RSS film (L_o*) was observed

to be 4.43 (Table 5). With the increase in the oxygen concentration from 1 to 2%, L_o* value significantly ($P < 0.05$) increased to 7.25. However, with further increase in oxygen concentration from 3 to 10% no significant change ($P > 0.05$) in L_o* values were observed. Up on photo-activation, the lightness value (L_p*) of film exposed to 1% oxygen significantly ($P < 0.05$) increased to 6.51. However, it can be seen that with the increase in oxygen content from 3 to 10% and photo-activation of the SC-MB-RSS films, non-significant ($P > 0.05$) differences were observed between the L_o* and L_p*. Furthermore, it was observed that the lightness value of the film exposed to 1% oxygen prior to photo-activation (L_o*) and exposed to ambient air after photo-activation (recovered) (L_r*) were similar ($P > 0.05$) indicating complete

Table 6 Effect of oxygen concentration on the instrumental colour values of original, photo-activated and colour-recovered CG-MB film

Oxygen concentration (%)[1]	Lightness (L^*)			Redness (a^*)			Blueness (b^*)		
	L_o^*	L_p^*	L_r^*	a_o^*	a_p^*	a_r^*	b_o^*	b_p^*	b_r^*
1 (0.45)	13.04 ± 1.20^{bA}	14.34 ± 1.28^{aB}	13.48 ± 1.32^{bAB}	4.24 ± 0.64^{aB}	0.85 ± 0.76^{aA}	4.12 ± 0.42^{aB}	-13.38 ± 0.65^{bA}	-11.35 ± 0.86^{aB}	-13.29 ± 0.86^{bA}
2 (2.27)	11.91 ± 0.76^{aA}	15.27 ± 1.10^{aB}	11.76 ± 1.17^{aA}	4.65 ± 0.88^{aB}	0.00 ± 1.03^{aA}	4.58 ± 0.87^{aB}	-13.91 ± 0.90^{aA}	-9.73 ± 0.77^{aB}	-14.24 ± 0.72^{aA}
3 (3.12)	11.72 ± 0.90^{aA}	15.80 ± 0.63^{aB}	11.72 ± 0.78^{aA}	4.76 ± 0.92^{aB}	0.24 ± 1.09^{aA}	4.38 ± 0.78^{aB}	-13.94 ± 0.74^{aA}	-9.82 ± 0.91^{aB}	-14.44 ± 0.78^{aA}
4 (4.21)	12.01 ± 1.16^{aA}	15.98 ± 0.87^{aB}	11.84 ± 0.71^{aA}	4.32 ± 0.52^{aB}	0.44 ± 1.13^{aA}	4.64 ± 0.89^{aB}	-13.88 ± 0.78^{aA}	-9.65 ± 0.88^{aB}	-14.32 ± 0.66^{aA}
5 (5.42)	12.01 ± 0.68^{aA}	16.00 ± 1.02^{aB}	11.86 ± 0.70^{aA}	4.44 ± 0.79^{aB}	0.21 ± 1.25^{aA}	4.53 ± 0.83^{aB}	-13.94 ± 0.98^{aA}	-9.76 ± 0.99^{aB}	-14.15 ± 0.50^{aA}
6 (6.10)	11.94 ± 1.20^{aA}	15.51 ± 0.85^{aB}	12.08 ± 0.67^{aA}	4.44 ± 0.87^{aB}	0.29 ± 1.23^{aA}	4.24 ± 0.83^{aB}	-13.82 ± 0.85^{aA}	-9.44 ± 0.90^{aB}	-14.12 ± 1.04^{aA}
7 (7.02)	11.94 ± 0.63^{aA}	15.76 ± 0.80^{aB}	11.94 ± 0.78^{aA}	4.53 ± 0.72^{aB}	0.38 ± 1.12^{aA}	4.74 ± 0.94^{aB}	-14.06 ± 0.91^{aA}	-9.62 ± 0.93^{aB}	-14.21 ± 0.78^{aA}
8 (8.26)	11.59 ± 0.68^{aA}	15.64 ± 0.71^{aB}	11.96 ± 0.54^{aA}	4.53 ± 0.74^{aB}	0.41 ± 1.13^{aA}	4.53 ± 0.86^{aB}	-13.94 ± 0.83^{aA}	-9.47 ± 0.92^{aB}	-14.5 ± 0.97^{aA}
9 (8.61)	11.89 ± 0.60^{aA}	15.56 ± 0.81^{aB}	11.79 ± 0.56^{aA}	4.65 ± 0.78^{aB}	0.32 ± 1.16^{aA}	4.62 ± 0.97^{aB}	-14.09 ± 0.83^{aA}	-9.61 ± 2.31^{aB}	-14.32 ± 0.73^{aA}
10 (10.10)	11.62 ± 0.79^{aA}	15.71 ± 0.88^{aB}	11.52 ± 0.66^{aA}	4.38 ± 0.65^{aB}	0.18 ± 1.05^{aA}	4.79 ± 0.81^{aB}	-14.09 ± 0.69^{aA}	-9.82 ± 0.94^{aB}	-14.18 ± 0.83^{aA}

Mean $\pm$ SD ($n = 16$)

[ABC]Values within a colour attribute (L^*, a^*, b^*) with at least one similar superscript do not differ significantly ($P > 0.05$)

[ab]Values within a column with at least one similar superscript do not differ significantly ($P > 0.05$)

[1]Values represent rounded concentration, while within the parenthesis, actual oxygen concentration is given

recovery of the colour. However, the same was not observed with increasing oxygen concentrations exposure (2–10%). Furthermore, some of the films took as high as 60 min to regain the original colour. It can be seen from Table 5 that significant differences ($P < 0.05$) in the redness values of the original SC-MB-RSS film (a_o^*) and the photo-activated SC-MB-RSS films (a_p^*) exist. Furthermore, it can be seen that up on exposure to ambient air, significant differences ($P < 0.05$) were observed between a_o^* and the redness values of the recovered films (a_r^*) indicating incomplete recovery of colour. Similar trends were observed in the original (b_o^*), photo-activated (b_p^*) and recovered (b_r^*) blueness values of SC-MB-RSS films. It can be seen from Table 5 that significant differences ($P < 0.05$) in the redness values of the original SC-MB-RSS film (a_o^*) and the photo-activated SC-MB-RSS films (a_p^*) exist. Furthermore, it can be seen that up on exposure to ambient air, significant differences ($P < 0.05$) were observed between a_o^* and the redness values of the recovered films (a_r^*) indicating incomplete recovery of colour. Similar trends were observed in the original (b_o^*), photo-activated (b_p^*) and recovered (b_r^*) blueness values of SC-MB-RSS films. b_o^* of the SC-MB-RSS film exposed to 1% oxygen was found to be -11.76 which decreased to -10.73, but the decrease was not significant ($P > 0.05$) statistically. The b^* values of all the films which were exposed to ambient air for recovery of original colour (b_r^*) remained almost same ($P > 0.05$) irrespective of exposure to initial oxygen concentration.

The colour values of CG-MB film exposed to different levels of oxygen and as affected by photo-activation and recovery are given in Table 6. The L^* values of the film prior to photo-activation (L_o^*) when exposed to 0.45% (1%)

oxygen were observed to be 13.04. With the increase in the oxygen concentration from 1 to 2%, L_o^* value significantly ($P < 0.05$) increased to 11.91. However, with further increase in oxygen concentration no significant changes ($P > 0.05$) were observed. Up on photo-activation, the L^* value (L_p^*) of film exposed to 1% oxygen significantly ($P < 0.05$) increased to 14.34. Furthermore, with an increase in the oxygen content from 2 to 10% and photo-activation of the CG-MB films, significant ($P < 0.05$) differences were observed between L_o^* and L_p^* (Table 6). The photo-activation time of CG-MB films ranged from 3 to 6 min while they took about 60 min to regain the original colour. It can be seen from Table 6 that significant differences ($P < 0.05$) in the redness values of the original (a_o^*) and the photo-activated CG-MB films (a_p^*) were observed at all oxygen levels of exposure. Furthermore, it can be seen that up on exposure to ambient air, non-significant differences ($P > 0.05$) were observed between a_o^* and the redness values of the recovered films (a_r^*) indicating complete recovery of redness. Similar trends were observed in the original (b_o^*), photo-activated (b_p^*) and recovered (b_r^*) blueness values of CG-MB films exposed to 1% oxygen concentration. The b_o^* of the CG-MB film exposed to 1% oxygen was found to be -13.38 which significantly ($P < 0.05$) decreased to -11.35 up on photo-activation (b_p^*). Up on exposure to ambient air the blueness value regained (b_r^*) and returned to original (-13.29). Similar trend was observed among the films exposed to increasing oxygen concentrations.

Mills and co-workers [43] reported that the initial rate of colour recovery (h^{-1}) was found dependent (linear variation) on oxygen concentration (0–100%). In addition, Lawrie and co-workers [33] reported that the recovery rate of

UV-activated colorimetric dye-based oxygen sensor was found to be directly proportional to the oxygen percentage in the headspace of the package. Mills and Lawrie [41] observed that there exists a linear relationship between the recovery time and the temperature during their studies on sulfonated polystyrene-based oxygen sensor containing MB, TiO_2, and glycerol. It was reported that the recovery time of the sensor was 5 days at room temperature and 7 days at 3.8 °C. Mills and co-workers [44] reported that oxygen indicator based on hydroxyl ethyl cellulose containing glycerol, TiO_2, indigo-tetrasulfonate was having a photo-activation time of less than 3 min in the absence of oxygen, while in ambient atmosphere, it was approximately 6 min. Khankaew and co-workers [29] reported that the total colour differences values and the initial rates of photo-activation of oxygen sensor film containing methyl cellulose were found to increase with increasing thickness; however, a decrease in photo-activation time was observed for a thickness of more than 106.67 μm. On the contrary, Mills and Lawrie [41] reported that the rate of recovery of sulfonated polystyrene-based oxygen sensor containing TiO_2, MB, and glycerol did not vary with changes in the film thickness but with the rate of diffusion of oxygen through the sensor film. Lawrie and co-workers [33] observed that the rate of recovery of hydroxyl ethyl cellulose based oxygen sensor containing MB, TiO_2 and glycerol was found to be proportional to percent oxygen and lower limit for oxygen sensitivity was 3%. Contrary to these reports, in the present study, it was observed that recovery rate was not dependent on the oxygen concentration in the headspace of the package.

Moisture Sorption Isotherms

The moisture sorption characteristics of the selected sensor films (SA-MB-NR, SC-MB-RSS, and CG-MB) was carried out using gravimetric method in the water activity (a_w) range of 0.11–0.92 at 25 °C involving sorbostats. The equilibrium moisture contents of all the sensor films across are shown in Fig. 4. The moisture sorption isotherms showed a slow initial increase in equilibrium moisture contents up to a_w 0.53 and thereafter a rapid increment in with further increase in a_w. All the three sensor films displayed non-linear behaviour. The moisture sorption curve of all the three sensor films was concave in shape, which is typical of water sensitive biopolymer film such as cellulose and gluten films [23]. The equilibrium moisture content of SA-MB-NR, SC-MB-RSS, and CG-MB films at a_w of 0.92 were observed to be 100.61, 94.73 and 120.26 g 100 g^{-1}, respectively, on dry basis. Fabra and co-workers [17] reported that glycerol as an ingredient in sodium caseinate-based sensor film promotes hygroscopic nature above 0.45 a_w. Shorter carbon chains and more number of hydroxyl and carboxylic groups also favour absorption of water (Kristo and Biliaderis [30]).
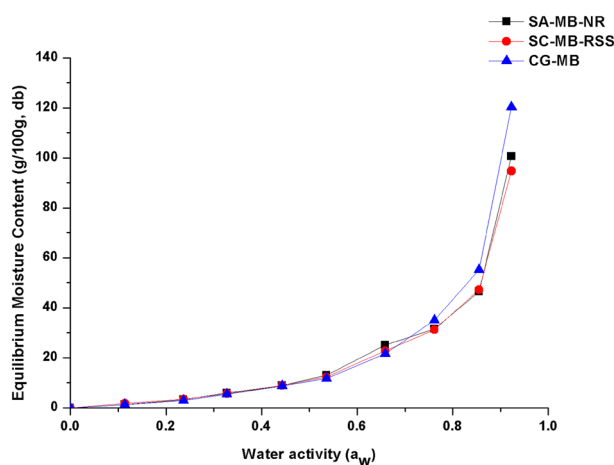

Fig. 4 Moisture sorption isotherms of different sensor films at 25 °C

Increasing rate of moisture absorption has also been reported with higher concentration of plasticizer [25]. The moisture sorption behaviour of the sensor films was described using four different mathematical models, namely, Ferro-Fontan, Peleg, D'Arcy, and Watt and Park models. The determined parameters of these sorption models and the goodness of fit of all the models are presented Table 7. Peleg model was best fitted for the experimental data of sodium alginate-based sensor film (SA-MB-NR) (Fig. 5a). The coefficient of determination (R^2) was found to be the highest (0.9980), while the reduced Chi square (χ^2) (2.00), percent mean deviation error (P) (5.49), and root mean square error percent (RMS%) (23.77) were the lowest among all other models. For both the sodium caseinate-based (SC-MB-RSS) (Fig. 5b) and carrageenan-based (CG-MB) (Fig. 5c) sensor films the D'Arcy and Watt model was found to best fit the observed values. In addition, the pattern of residuals (the difference between the observed and predicted values) was randomly arranged. Several authors had reported that the moisture sorption of most protein based films such as whey protein [13], sodium caseinate–lipid [16], soy protein [18] and sodium caseinate–pullulan [31] are sigmoid in shape with a characteristic type II isotherm. Lim and co-workers [35, 36] observed similar results in transglutaminase cross-linked egg white protein and gelatin films and reported concave shape of sorption curves might be due to the development of water masses in the polymer matrix with increasing water activity. Swelling of the polymer matrix causes exposure of more binding sites for water sorption due to which EMC increased at a rapid rate in later stages. Galus and Lenart [21] reported sigmoidal shape for sodium alginate and pectin based antimicrobial films and best fitted model was Peleg model with minimum mean relative error (P) of 3.510. An increase in number of hydrogen bonds prevents the diffusion of water molecules through protein films and

Table 7 Estimated values of sorption model parameters at 25 °C

Model	Parameter	SA-MB-NR	SC-MB-RSS	CG-MB
Ferro-Fontan (a_w = 0.1–0.9)	A	0.99	1.01	1.01
	B	9.68	7.36	5.89
	C	1.07	0.97	0.89
	R^2	0.9876	0.9932	0.9964
	χ^2	12.38	6.12	5.37
	P	9.22	23.87	27.77
	RMS%	79.62	38.14	49.82
Peleg (a_w = 0.1–0.9)	A	593.31	55.57	423.92
	B	58.47	319.69	65.66
	C_1	30.51	2.20	23.11
	C_2	2.21	23.65	2.54
	R^2	0.9980	0.9984	0.9984
	χ^2	2.00	1.49	2.38
	P	5.49	16.05	20.42
	RMS%	23.77	28.07	32.52
D'Arcy and Watt (a_w = 0.1–0.9)	K_1	− 1.02	0.14	− 2.95E−7
	K_2	1.62	− 1820.21	0.0048
	K_3	15.34	272.33	6.13
	K_4	1.02	1.04	1.01
	K_5	6.69	2.64	8.16
	R^2	0.9890	0.9984	0.9969
	χ^2	10.99	1.47	4.53
	P	10.14	11.23	12.44
	RMS%	39.46	19.72	17.12
Park (a_w = 0.1–0.9)	A	− 7.11	− 3032.47	− 6.05
	B	2.49E45	0.143	− 3.73E46
	H	44.06	428.80	39.09
	K	15.67	13.22	19.65
	n	17.96	21.02	14.08
	R^2	0.9855	0.9972	0.9894
	χ^2	14.50	2.49	15.69
	P	12.69	16.74	36.71

R^2: coefficient of determination; χ^2: reduced Chi square; P: percent mean deviation error; RMS%: root mean square error percent; A, B, C, C_1, C_2, H, K_1, K_2, K_3, K_4, and K_5 are model parameters

it also delays the transport of diffusing species [37]. Sodium ions might also be the reason for higher rate of water absorption because they create regions of high dielectric constant suitable for water absorption [15]. Non-linear nature of water sorption of sensor films could be due to structural changes caused by absorption of water at hydrophilic sites [12]. Alves and co-workers [2] reported GAB model as best fit model for carrageenan/pectin films with mica flakes. The moisture sorption was having a sigmoidal shape with sharp rise in moisture content after a water activity of 0.6. Due to interaction between different components and change in morphology of the films, altered moisture sorption curves were obtained for increasing concentration of mica flakes. Moisture sorption of agar/k-carrageenan/glucomannan was having sigmoidal shape with rapid increase after 0.7 a_w.

Conclusion

The present study attempted to develop and characterize the properties of sodium alginate (SA-MB-NR), sodium caseinate (SC-MB-RSS) and carrageenan (CG-MB) based oxygen leak indicators for food-packaging applications. All the three sensor films were found to be equally sensitive to oxygen concentration ranging from 1 to 10%. At the lowest oxygen concentration (1%), the instrumental colour values (L^*, a^*, b^*) of all the three sensor films prior to photo-activation (original) were significantly ($P < 0.05$) different from the rest of the concentrations. SA-MB-NR and SC-MB-RSS were found to have very high migration into all the food simulants except in n-heptane. In contrast, the CG-MB sensor film was having the least overall migration into all food simulants.
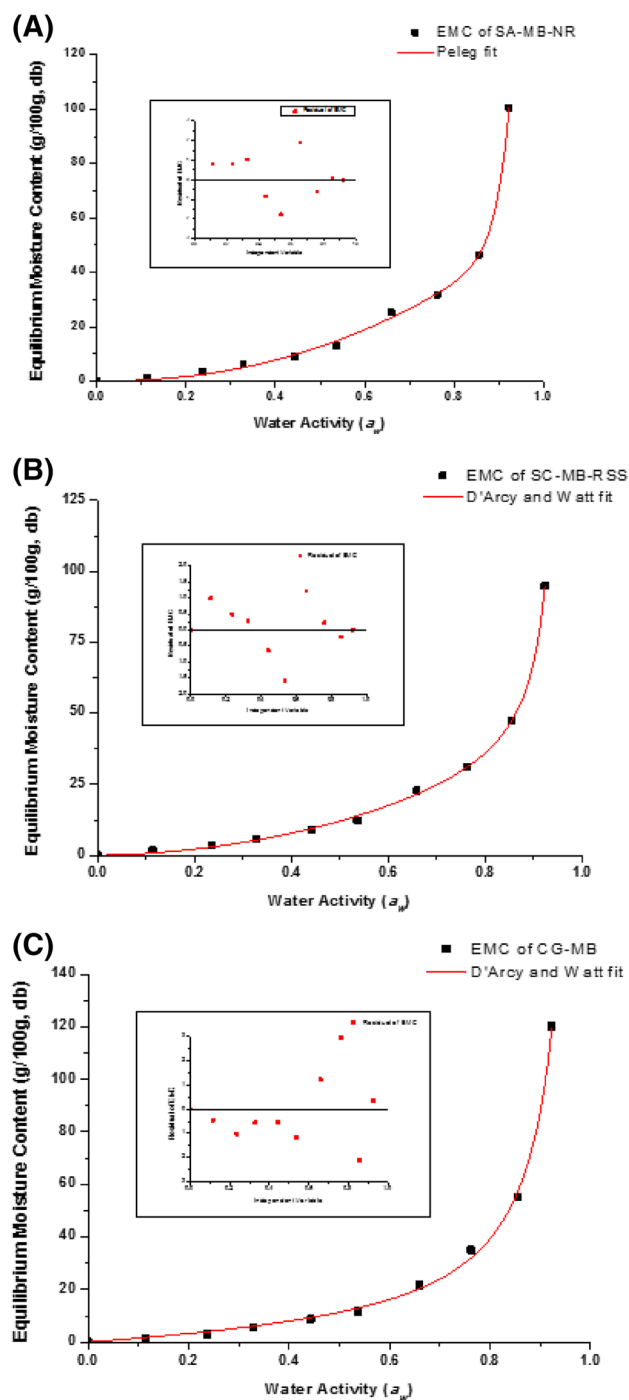
Fig. 5 Best fitting moisture sorption model and pattern of residuals for different sensor films at 25 °C. **a** SA-MB-NR, **b** SC-MB-RSS, **c** CG-MB

No significant difference in the mechanical properties of the sensor films was found among the sensor films ($P > 0.05$). FTIR spectra of SA-MB-NR and SC-MB-RSS revealed a change due to UV activation between the wavenumbers 2300–2500 cm^{-1}, which corresponds to alkyl and amide bond changes. While the spectra of CG-MB film showed

a change between 2300 and 3900 cm^{-1} wave numbers that corresponded to the stretching of hydroxyl groups. Sorption isotherms of all the three films resembled type-III according to the BET classification. Peleg model was found to best describe the moisture sorption behaviour of SA-MB-NR sensor films while *D'Arcy and Watt model* best described the sorption behaviour of SC-MB-RSS and CG-MB films. Hence, it can be concluded that carrageenan-based sensor film (CG-MB) could be potentially applied as an oxygen leak indicator for direct contact (vacuum) or non-direct contact (modified atmosphere) food-packaging applications.

References

1. Abad LV, Kudo H, Saiki S, Nagasawa N, Tamada M, Katsumura Y, De La Rosa AM (2009) Radiation degradation studies of carrageenans. Carbohydr Polym 78(1):100–106
2. Alves VD, Costa N, Coelhoso IM (2010) Barrier properties of biodegradable composite films based on kappa-carrageenan/pectin blends and mica flakes. Carbohydr Polym 79(2):269–276
3. Arrieta MP, Peltzer MA, del Carmen Garrigos M, Jimenez A (2013) Structure and mechanical properties of sodium and calcium caseinate edible active films with carvacrol. J Food Eng 114(4):486–494
4. ASTM (1992) Standard test methods for tensile properties of thin plastic sheeting. Annual book of ASTM standards. American Society for Testing of Materials, Philadelphia, pp 313–321
5. Audic JL, Chaufer B (2005) Influence of plasticizers and crosslinking on the properties of biodegradable films made from sodium caseinate. Eur Polym J 41(8):1934–1942
6. Avena-Bustillos RJ, Krochta JM (1993) Water vapour permeability of caseinate based edible films as affected by pH, calcium cross-linking and lipid content. J Food Sci 58(4):904–907
7. Belbekhouche S, Bras J, Siqueira G, Chappey C, Lebrun L, Khelifi B, Marias S, Dufresne A (2011) Water sorption behavior and gas barrier properties of cellulose whiskers and microfibrils films. Carbo Polym 83(4):1740–1748
8. BCC Research (2013) The advanced packaging solutions market value for 2017 is projected to be nearly $44.3 billion. http://www.bccresearch.com/pressroom/food/advanced-packaging-solutions-market-value-projected-nearly-$44.3-billion-2017. Accessed on 26 Nov 2017
9. Biji KB, Ravishankar CN, Mohan CO, Gopal TKS (2015) Smart packaging systems for food applications: a review. J Food Sci Technol 52(10):6125–6135
10. Brody AL, Strupinsky EP, Kline LR (2001) Active packaging for food applications. CRC Press, Massachusetts
11. Cha DS, Choi JH, Chinnan MS, Park HJ (2002) Antimicrobial films based on Na-alginate and κ-carrageenan. LWT-Food Sci Technol 35(8):715–719
12. Chen CH, Kuo WS, Lai LS (2009) Effect of surfactants on water barrier and physical properties of tapioca starch/decolorized hsian-tsao leaf gum films. Food Hydrocoll 23(3):714–721

13. Coupland JN, Shaw NB, Monahan FJ, O'Riordan ED, O'Sullivan M (2000) Modeling the effect of glycerol on the moisture sorption behaviour of whey protein edible films. J Food Eng 43:25–30

14. D'Arcy RL, Watt, IC (1970) Analysis of sorption isotherms of non-homogeneous sorbents. Trans Fara Soc 66:1236–1245

15. Eisenberg A, Navratil M (1973) Ion clustering and viscoelastic relaxation in styrene-based ionomers. II. Effect of ion concentration. Macromolecules 6(4):604–612

16. Fabra MJ, Perez-Masia R, Talens P, Chiralt A (2011) Influence of the homogenization conditions and lipid self-association on properties of sodium caseinate based films containing oleic and stearic acids. Food Hydrocoll 25(5):1112–1121

17. Fabra MJ, Talens P, Chiralt A (2010) Water sorption isotherms and phase transitions of sodium caseinate-lipid films as affected by lipid interactions. Food Hydrocoll 24(4):384–391

18. Fletouris DJ, Govari MA, Botsoglou EN (2015) The influence of retail display storage on the fatty acid composition of modified atmosphere packaged Graviera Agraphon cheese. Int J Dairy Technol 68(2):218–226

19. Fontan CF, Chirife J, Sancho E, Iglesias HA (1982) Analysis of a model for water sorption phenomena in foods. J Food Sci Technol, 47(5):1590–1594

20. Francis FJ, Clydesdale FM (1975) Food colorimetry: theory and applications. AVI Publishing Co., Inc., Westport

21. Galus S, Lenart A (2013) Development and characterization of composite edible films based on sodium alginate and pectin. J Food Eng 115(4):459–465

22. Ghayal G, Jha A, Kumar A, Gautam AK, Rasane P (2015) Effect of modified atmospheric packaging on chemical and microbial changes in dietetic rabri during storage. J Food Sci Technol 52(3):1825–1829

23. Gontard N, Guilbert S, Cuq JL (1993) Water and glycerol as plasticizers affect mechanical and water vapor barrier properties of an edible wheat gluten film. J Food Sci 58(1):206–211

24. Hempel AW, O'Sullivan MG, Papkovsky DB, Kerry JP (2013) Use of smart packaging technologies for monitoring and extending the shelf life quality of modified atmosphere packaged (MAP) bread: application of intelligent oxygen sensors and active ethanol emitters. Eur Food Res Technol 237:117–124

25. Hernandez-Munoz P, Kanavouras A, Perry KWN, Gavara R (2003) Development and characterization of biodegradable films made from wheat gluten protein fractions. J Agric Food Chem 51:7647–7654

26. IS 9845 (1998) Determination of overall migration of constituents of plastics materials and articles intended to come in contact with foodstuffs—methods of analysis. Indian Standard. Bureau of Indian Standards, New Delhi

27. Jain V, Rasane P, Jha A, Sharma N, Gautam A (2015) Effect of modified atmospheric packaging on the shelf life of kalakand and its influence on microbial, textural, sensory and physico-chemical properties. J Food Sci Technol 52(7):4090–4101

28. Jha A, Kumar A, Jain P, Gautam AK, Rasane P (2015) Effect of modified atmosphere packaging on the shelf life of lal peda. J Food Sci Technol 52(2):1068–1074

29. Khankaew S, Boonsupthip W, Nandhivajrin C, Suppakul P (2015) Effect of thickness and pH on color transition of a novel UVA-activated oxygen bio-indicator. In: 27th IAPRI symposium on packaging, Thailand

30. Kristo E, Biliaderis CG (2007) Physical properties of starch nanocrystal-reinforced pullulan films. Carbohydr Polym 68:146–158

31. Kristo E, Koutsoumanis KP, Biliaderis CG (2008) Thermal, mechanical and water vapor barrier properties of sodium caseinate films containing antimicrobials and their inhibitory action on Listeria monocytogenes. Food Hydrocoll 22(3):373–386

32. Kumari A, Emerald E, Magdaline F, Simha V, Pushpadass HA (2015) Effects of baking conditions on colour, texture and crumb grain characteristics of Chhana Podo. Int J Dairy Technol 68(2):270–280

33. Lawrie K, Mills A, Hazafy D (2013) Simple inkjet-printed, UV-activated oxygen indicator. Sens Actuators B 176:1154–1159

34. Lee SK, Sheridan M, Mills A (2005) Novel UV-activated colorimetric oxygen indicator. Chem Mater 17(10):2744–2751

35. Lim LT, Mine Y, Tung MA (1998) Transglutaminase cross-linked egg white protein films: tensile properties and oxygen permeability. J Agric Food Chem 46(10):4022–4029

36. Lim LT, Mine Y, Tung MA (1999) Barrier and tensile properties of transglutaminase cross-linked gelatin films as affected by relative humidity, temperature, and glycerol content. J Food Sci 64(4):616–622

37. Marcovich NE, Auad ML, Bellesi NE, Nutt SR, Aranguren MI (2006) Cellulose micro/nanocrystals reinforced polyurethane. J Mater Res 21(04):870–881

38. Mastromatteo M, Conte A, Lucera A, Saccotelli MA, Buonocore GG, Zambrini AV, Nobile MAD (2015) Packaging solutions to prolong the shelf life of Fiordilatte cheese: bio-based nanocomposite coating and modified atmosphere packaging. LWT-Food Sci Technol 60(1):230–237

39. Mihailović D, Šaponjić Z, Radoičić M, Radetić T, Jovančić P, Nedeljković J, Radetić M (2010) Functionalization of polyester fabrics with alginates and TiO_2 nanoparticles. Carbohydr Polym 79(3):526–532

40. Mills A (2005) Oxygen indicators abd intelligent inks for packaging food. Chem Soc Rev 34(12):1003–1011

41. Mills A, Lawrie K (2011) Novel photocatalyst-based colorimetric indicator for oxygen: use of a platinum catalyst for controlling response times. Sens Actuators B 157(2):600–605

42. Mills A, McGrady M (2008) A study of new photocatalyst indicator inks. J Photochem Photobiol A 193(2):228–236

43. Mills A, Hazafy D, Lawrie K (2011) Novel photocatalyst-based colorimetric indicator for oxygen. Catal Today 161(1):59–63

44. Mills A, Tommons C, Bailey RT, Tedford MC, Crilly PJ (2008) UV-activated luminescence/colorimetric O_2 indicator. Int J Photoenergy 2008:81–87

45. Morren S, Ho QT, Stoops J, Dyck TV, Claes J, Verboven P, Nicolai B, Campenhout LV (2017) Effect of product microstructure and process parameters on modified atmosphere packaged bread. Food Bioprocess Technol 10:328–339

46. Nielsen SS (2002) Introduction to the chemical analysis of foods. CBS Publishers and Distributors, New Delhi, pp 341–347

47. O'Mahony FC, O'Riordan TC, Papkovskaia N, Kerry JP, Papkovsky DB (2006) Non-destructive assessment of oxygen levels in industrial modified atmosphere packaged cheddar cheese. Food Control 17(4):286–292

48. Panjagari NR, Singh AK, Ganguly S, Indumati KP (2015) Beta-glucan rich composite flour biscuits: modelling of moisture sorption isotherms and determination of sorption heat. J Food Sci Technol 52(9):5497–5509

49. Paşcalău V, Popescu V, Popescu GL, Dudescu MC, Borodi G, Dinescu A, Paul M (2012) The alginate/k-carrageenan ratio's influence on the properties of the cross-linked composite films. J Alloys Compd 536:S418–S423

50. Peleg M (1993) Assessment of a semi-empirical four parameter general model for sigmoid moisture sorption isotherms. J Food Pro Eng 16(1):21–37

51. Pereda M, Amica G, Rácz I, Marcovich NE (2011) Structure and properties of nanocomposite films based on sodium caseinate and nanocellulose fibers. J Food Eng 103:76–83

52. Pereda M, Aranguren MI, Marcovich NE (2008) Characterization of chitosan/caseinate films. J Appl Polym Sci 107(2):1080–1090

53. Ramamoorthy R, Dutta PK, Akbar SA (2003) Oxygen sensors: materials, methods, designs and applications. J Mater Sci 38(21):4271–4282

54. Restuccia D, Spizzirri UG, Parisi OI, Cirillo G, Curcio M, Iemma F, Picci N (2010) New EU regulation aspects and global market of active and intelligent packaging for food industry applications. Food Control 21(11):1425–1435

55. Rhim JW (2004) Physical and mechanical properties of water resistant sodium alginate films. LWT-Food Sci Technol 37(3):323–330

56. Rhim JW (2012) Physical-mechanical properties of agar/k-carrageenan blend film and derived clay nanocomposite film. J Food Sci 77(12):N66–N73

57. Robertson GL (2013) Food packaging: principles and practice. CRC Press, Boca Raton

58. Shearer SA, Payne FA (1990) Color and defect sorting of bell peppers using machine vision. Trans Am Soc Agric Biol Eng 33(6):1245–1250

59. Shojaee-Aliabadi S, Hosseini H, Mohammadifar MA, Mohammadi A, Ghasemlou M, Hosseini SM, Khaksar R (2014) Characterization of κ-carrageenan films incorporated plant essential oils with improved antimicrobial activity. Carbohydr Polym 101:582–591

60. Siew DC, Heilmann C, Easteal AJ, Cooney RP (1999) Solution and film properties of sodium caseinate/glycerol and sodium caseinate/polyethylene glycol edible coating systems. J Agric Food Chem 47(8):3432–3440

61. Smiddy M, Fitzgerald M, Kerry JP, Papkovsky DB, O'Sullivan CK, Guilbault GG (2002) Use of oxygen sensors to non-destructively measure the oxygen content in modified atmosphere and vacuum packed beef: impact of oxygen content on lipid oxidation. Meat Sci 61(3):285–290

62. Smiddy M, Papkovskaia N, Papkovsky DB, Kerry JP (2002) Use of oxygen sensors for the non-destructive measurement of the oxygen content in modified atmosphere and vacuum packs of cooked chicken patties; impact of oxygen content on lipid oxidation. Food Res Int 35(6):577–584

63. Tavassoli-Kafrani E, Shekarchizadeh H, Masoudpour-Behabadi M (2016) Development of edible films and coatings from alginates and carrageenans. Carbohydr Polym 137:360–374

64. Thippeswamy L, Venkateshaiah BV, Patil SB (2011) Effect of modified atmospheric packaging on the shelf life stability of paneer prepared by adopting hurdle technology. J Food Sci Technol 48(2):230–235

65. Vu CHT, Won K (2013) Novel water-resistant UV-activated oxygen indicator for intelligent food packaging. Food Chem 140(1):52–56

66. Vu CHT, Won K (2014) Leaching-resistant carrageenan-based colorimetric oxygen indicator films for intelligent food packaging. J Agric Food Chem 62(29):7263–7267

67. Wang L, Auty MA, Kerry JP (2010) Physical assessment of composite biodegradable films manufactured using whey protein isolate, gelatin and sodium alginate. J Food Eng 96(2):199–207

68. Yam KL, Takhistov PT, Miltz J (2005) Intelligent packaging: concepts and applications. J Food Sci 70(1):1–10

69. Yin YJ, Yao KD, Cheng GX, Ma JB (1999) Properties of polyelectrolyte complex films of chitosan and gelatin. Polym Int 48(6):429–432